A&A 439, 323–334 (2005)
DOI: 10.1051/0004-6361:20052879

Astronomy & Astrophysics

Numerical modeling of solar faculae close to the limb

O. V. Okunev[1,2] and F. Kneer[1]

[1] Institut für Astrophysik, Friedrich-Hund-Platz 1, 37077 Göttingen, Germany
e-mail: olok@uni-sw.gwdg.de
[2] Central Astronomical Observatory at Pulkovo, 196140 St. Petersburg, Russia

Received 15 February 2005 / Accepted 4 May 2005

Abstract. A numerical simulation was performed to interpret high-resolution spectropolarimetric observations of polar faculae on the Sun. A semi-empirical three-dimensional model of facula structures, controlled by several free parameters, was constructed. It consists of two components, the atmosphere within small-scale magnetic flux tubes and the exterior atmosphere. Multi-ray 1.5D radiative transfer calculations were performed along oblique rays passing through a highly inhomogeneous atmosphere of the simulation box. By the comparison of the properties of the calculated Stokes profiles from the synthetic faculae with the observed properties, a set of free parameters of the model (such as: size, number density of flux tubes, internal temperature stratification and magnetic field strength) was deduced, which satisfies the observational constraints. The hypothesis about solar faculae as a conglomerate of small-scale magnetic flux tubes is verified. The model reproduces all observed properties: the continuum contrast and its center-to-limb variation, the Stokes I and V profiles of Fe I and Fe II lines, the apparent magnetic field strengths, and the displacement towards the limb of the continuum intensity against the line-of-sight magnetograms.

Key words. Sun: faculae, plages – Sun: magnetic fields – methods: numerical – radiative transfer

1. Introduction

The polar areas of the Sun take part in the magnetic activity cycle, as do activity regions at low latitudes of the Sun. During sunspot minimum, small brightenings appear at heliographic latitudes $|\phi_\odot| \geq 60°$. They are called polar faculae (henceforth PFe) and have apparent sizes of a few arcsec. For the successful study of such small-scale magnetic structures close to the solar limb one has to combine high spectral and spatial resolution spectropolarimetric observations with efficient methods of data analysis and interpretation including numerical simulations.

In a preceding observational study of PFe we had obtained a wealth of information about the structure and dynamics of facular atmospheres (Okunev & Kneer 2004, hereafter referred as Paper I). There, spectropolarimetric properties of PFe such as intensity distribution (brightness contrast and its center-to-limb variation – CLV), sizes and fine structure, dynamics, characteristics of the intensity profiles and polarimetric signals in three iron lines (Fe I 6301.5 Å, 6302.5 Å and Fe II 6149.3 Å) were collected. The difficulty in treating weak polarimetric signals from positions close to the solar limb was overcome, in part, by the application of sophisticated mathematical methods of data reduction and analysis. The present contribution deals with the modeling of faculae to obtain their physical properties.

With standard calibrations one can only approximately estimate average values of the facular atmospheric parameters. Most methods of data interpretation are based on several simplifications (such as a plane parallel atmosphere) that are not necessarily fulfilled in the solar photosphere. This holds especially for observations close to the limb, where the photosphere is very inhomogeneous along the line-of-sight (LOS). It can lead to incorrect estimates of the parameters. The importance of the detailed geometry of rays crossing very intermittent magnetic fields was shown by Solanki et al. (1998).

The result of the interpretation depends also on the adopted assumptions. For example the calibration of magnetograms depends strongly on the chosen approximation: weak field or strong field. Generally, we do not know a priori which one is appropriate. Furthermore, the area filling factor and the inclination of the magnetic field are two more unknown factors, which make the interpretation of the polarimetric observations even more difficult.

One solution is to apply numerical methods involving radiative transfer calculations, such as, for example, inversions of Stokes profiles (e.g. Ruiz Cobo & del Toro Iniesta 1992). This has been successfully applied to a wide range of problems in physics of the solar photosphere (e.g. Bellot Rubio et al. 2000; Borrero & Bellot Rubio 2002; Puschmann et al. 2005). Yet, this technique demands high quality data (high spectral resolution and high SNR). Usually, the inversion technique is a pure 1D approach; each single ray is considered independently and under the assumption of plane-parallel atmospheres a 1D radiative transfer problem is solved. Furthermore, to avoid time-consuming calculations and for convergence of the iterations only a small number of nodes (reference grid points along the

integration path) are used for adjustment of the guess model. This peculiarity of the method makes it difficult to apply it to problems where the atmosphere along the LOS is very irregular and high coverage with grid points is mandatory. The formation of a magnetically-sensitive line close to the solar limb is characterized by a very intermittent atmosphere along the LOS, which requires many grid points along the integration path.

For this study, we have chosen another approach known as forward modeling. The idea is to create a physical semi-empirical model, controlled by several free parameters, to calculate emergent Stokes profiles $\boldsymbol{I}_{\rm syn}(x', y', \lambda)$ for several sets of the free parameters and to compare them with the observed profiles. The advantage of the forward modeling is that one can create a realistic two- or even three-dimensional model and test its viability. The calculations can be performed with any required spatial resolution, both in directions along the LOS and perpendicular to it.

Numerical modeling and radiative transfer calculations of the magnetic structures at large heliocentric angles with the LOS oblique to the axis of magnetic flux tubes (MFTs) have several peculiarities, which were discussed by Audic (1991), Bünte et al. (1993) and Solanki et al. (1998), who have performed such modeling. Keller et al. (2004) have used the MURaM code of the Lindau-Chicago group (Vögler & Schüssler 2003; Vögler et al. 2005), which solves numerically the complete set of the time-dependent magneto-hydrodynamic equations together with non-gray radiative transfer. They obtained good agreement with the observations of solar faculae by Lites et al. (2004). These observations and simulations were restricted to continuum intensities at $\cos\theta = 0.5$ (and $\cos\theta = 0.88$ in the simulations).

Radiative transfer calculations across flux tubes were also performed by Karpinsky & Okunev (1998) to explain the observed fine structure of the brightness at the extreme limb of the Sun (Karpinsky & Okunev 1997). The latter calculations were limited to the continuum intensity. In this work we extend the modeling to the radiative transfer of the full Stokes vector in order to interpret the high resolution spectropolarimetric observations of the facular structures at the solar poles. The aim of the study was not to find parameters of the atmosphere which give a best fit of individual line profiles, but to verify the hypothesis about PFe as concentrations of small-scale MFTs and to find the most adequate set of free parameters which will be able to reproduce the typical portrait of PFe, given by average observed properties of PFe.

Our work has potential relevance for faculae in general. Yet, as is seen in G-band observations presented, e.g., by Keller et al. (2004) and by Carlsson et al. (2004), many faculae are single-structured, in as far as today's (excellent) spatial resolution can establish. PFe are somewhat different, with their size of $1-2''$. They dissolve at high spatial resolution into a conglomerate of nearby bright structures. The emphasis of the present study is to simulate these conglomerates of magnetic flux tubes.

The next section describes the basic assumptions and principles of the performed numerical modeling. Section 3 presents result of simulations in comparison with the apparent properties of PFe derived in Paper I, and Sect. 4 concludes the paper.

2. Construction of the model

2.1. Basic assumptions

The magnetic inhomogeneity of the facular atmosphere is modeled by static magnetic flux tubes (MFTs) embedded in a field free medium. Such an assumption is supported by the observed properties of polar faculae. PFe were found to have fine structure both in magnetic field and intensity contrast and are characterized by kilo-Gauss fields and weak average flux density (Paper I). The latter is due to the limited spatial resolution of the observations (small filling factors). Accordingly, the magnetic elements possess only very small diameters.

Thus, the model consists of two components: magnetic and non-magnetic, or internal and external with respect to the MFT. The components differ not only in the presence/absence of magnetic field but also in physical conditions, such as temperature, gas pressure, electron pressure, opacity, etc. For the external non-magnetic atmosphere we adopt the VALC model (Vernazza et al. 1981) extended to deeper subphotospheric layers using the model of the convective zone of Spruit (1977). The model covers a range of heights in the solar atmosphere from $z = -200$ km to 600 km, where $z = 0$ refers, as usually, to continuum optical depth $\tau_{\rm c} = 1$ at $\lambda = 5000$ Å. The parameters of the internal atmosphere are given by the prescribed thermal stratification (parameter of the model) and the gas pressure obtained from the pressure balance between the magnetic and non-magnetic atmospheres (cf. Eq. (1) below). The magnetic structure of the internal atmosphere is defined by the adopted model of the magnetic flux tube (MFT).

Although it was found from observations that polar faculae are highly dynamic structures of the solar photosphere, we restrict our modeling to the static case for simplicity. We adopt stationary MFTs in pressure balance with the external atmosphere. Modeling of the shifts and asymmetries of Stokes I and V profiles are deferred to forthcoming studies, and the present work deals with photometric contrasts, line strengths and amplitudes of polarimetric signals.

2.2. Model of a single magnetic flux tube

The concept of small-scale MFTs as bricks which constitute unresolved magnetic fields in the solar atmosphere is a cornerstone of the presented numerical model. The adopted model assumptions are the usual for such calculations: axisymmetric vertical flux tubes are in pressure balance with the surrounding photosphere; the parameters of the internal atmosphere $(T, P_{\rm g})$ depend only on height and not on radius (thin tube approximation).

The external gas pressure is balanced by the internal gas and magnetic pressures, which yields within the thin flux tube approximation

$$P_{\rm g}^{\rm ext}(z) = P_{\rm g}^{\rm int}(z) + \frac{B^2(z)}{8\pi}. \quad (1)$$

Magnetic fields of flux tubes are predominantly vertical in the lower photosphere, and for the z component of the field we assume:

$$B_z(z) = B_0 {\rm e}^{-z/2H_p(z)}, \quad (2)$$

where B_0, the magnetic field strength at $z = 0$ is a free parameter of the model, and $H_p(z)$ is the pressure scale height, which was taken from the external pressure stratification. Fixing thus $B(z)$ and having prescribed $P^{\rm ext}(z)$ the internal pressure was found from Eq. (1). Tests have shown that this $P^{\rm int}(z)$ satisfies closely the condition of hydrostatic equilibrium $\mathrm{d}p = -\rho\, g\, \mathrm{d}z$ for the adopted thermal model (Sect. 2.5).

The second parameter of the model is the radius (R_0) of the MFT at $z = 0$. From the law of magnetic flux conservation $R(z)^2 B(z) = R_0^2 B_0$ together with Eq. (2) we can find the expansion of the flux tube:

$$R(z) = R_0 \sqrt{\frac{B_0}{B(z)}}. \tag{3}$$

Flux tubes are not strictly cylindrical; they are expanding upwards. Therefore, it will be more appropriate to describe the magnetic field vector in cylindrical coordinates with two components, the vertical B_z and the radial B_r. The azimuthal component B_ϕ is set to zero. To obtain B_r we proceed in a way similar to Audic (1991). We assume that at the axis of a tube the magnetic field is strictly vertical and the radial component vanishes ($|B(r = 0)| = B_z$), and at the boundary ($r = R_0$) of the MFT the direction of the magnetic field vector $\boldsymbol{B} = (B_r, B_z)$ is given by the radial expansion of the tube (Fig. 1). Between the axis and the boundary we assume a linear behavior of the radial component

$$B_r(r, z) = B_z(z) \frac{r}{R_0} \frac{\mathrm{d}R(z)}{\mathrm{d}z}. \tag{4}$$

The radial component $B_r(r, z)$, introduced in such a way, is the only deviation from the thin flux tube approximation. Other physical parameters of the internal atmosphere are functions of the height only. It can easily be seen that the adopted components B_r and B_z satisfy the condition $\mathrm{div}\boldsymbol{B} = 0$.

Thus, R_0 and B_0 are the two free parameters which fully define the geometry and magnetic field configuration of a single flux tube. Typical values of these parameters to be used in the model are 100 km and 1400 G, respectively. The corresponding magnetic flux then is $\Phi = 4.4 \times 10^{17}$ Mx.

The dependence, defined by Eq. (3), implies infinite expansion of a tube with height. Yet, such a configuration leads to the intersection at certain heights with the fields of neighboring flux tubes. It is generally believed that MFTs while expanding upwards merge and form a so-called *magnetic canopy*. Pneuman et al. (1986) have derived a tube model in which they also considered the merging of flux tubes. In our case, in order to avoid ambiguity caused by the intersection of the MFTs we have restricted the expansion of the flux tube, introducing the maximum radius which it can reach (Fig. 1). The latter depends on the merging height, which in turn depends on the number density of MFTs on the surface, or number of tubes in the simulation box.

2.3. Construction of the 3D box and multiple rays

A full 3D model was constructed with the vertical size $Z_{\rm s}$, given by the range of heights of the photospheric model, and with the horizontal extent of the box $X_{\rm s} = 3''$ and $Y_{\rm s} = 2''$, where

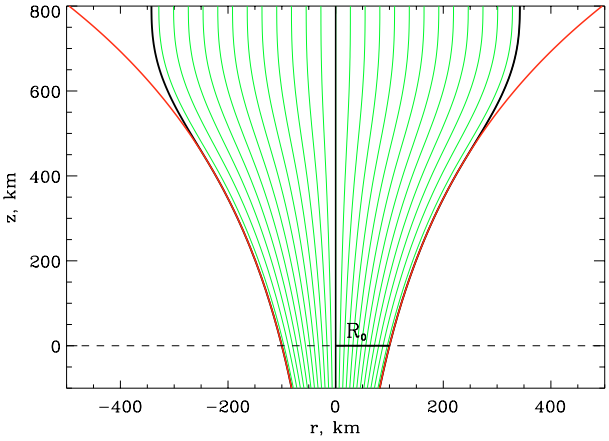

Fig. 1. Axial section of the MFT in the XZ plane illustrating the configuration of the magnetic field of the flux tubes. Model parameter $R_0 = 100$ km. The expansion of the magnetic flux tube is limited by the introduced largest attainable radius $R_{\rm max} = 300$ km.

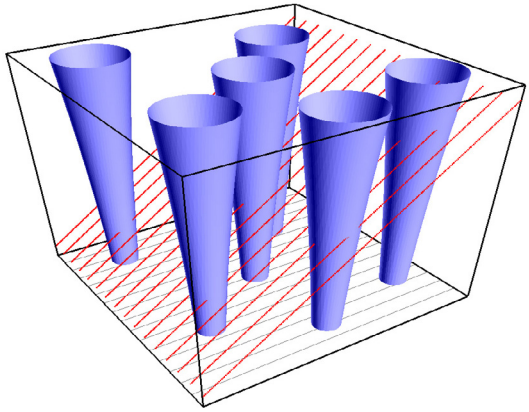

Fig. 2. 3D simulation box populated with isolated MFTs crossed by an array of parallel rays, schematically.

the Y axis is parallel to the limb and structures in this direction will not show perspective foreshortening close to the limb, and the X axis is perpendicular to the limb. The chosen size of the simulation box was inspired by the observed facular shapes and sizes (Paper I). Accounting for the limb effects the chosen size of the simulation box approximately correspond to the observed sizes of PFe in the directions parallel and perpendicular to the limb.

Next, the simulation box was populated with identical MFTs (Fig. 2) randomly distributed on the surface (XY plane at $z = 0$ km). To study the effect of many flux tubes along the LOS at large heliocentric angles, we have used three realizations of the MFT distribution in the simulation box (hereafter referred to as distribution N1, N2 and N3), which differ only in the number of MFTs in the box (Table 1).

We have introduced the filling factor of the model $f_{\rm mod}$ defined as the ratio of the area occupied by the flux tubes at $z = 0$ km to the total area of the simulation box:

$$f_{\rm mod} = \frac{\pi R_0^2 N_{\rm MFT}}{S_{\rm box}}.$$

Table 1. Three realizations of the random MFT distribution in the simulation box.

Distribution	$N_{\rm MFT}$ in the box	$f_{\rm mod}$
N1	5	0.05
N2	11	0.1
N3	21	0.2

The values of $f_{\rm mod}$ are given in Table 1 assuming $R_0 = 100$ km, a typical value of the parameter R_0, which however can be varied resulting in changes of the filling factor.

For the 3D simulation box thus constructed a radiative transfer problem was solved for various inclinations of the LOS to the vertical direction Z, corresponding to observations at different heliocentric angles. To obtain the center-to-limb variation the calculations were performed at several inclinations $\mu = \cos\theta = (1., 0.8, 0.6, 0.4, 0.2, 0.1)$. For each μ an array of parallel rays was introduced along which the integrations were performed as shown in Fig. 2. Each ray crosses several inhomogeneities along the LOS resulting from the non plane-parallel atmosphere of the 3D box, but the RT calculations are performed separately for each ray and independently from the other rays. Such an approach is called 1.5D radiative transfer.

The detailed geometry of each ray passing the flux tubes was considered exactly:

- the rays do not necessarily pass through the axis of the MFTs (Fig. 3a);
- the rays cross the MFTs at various heights in the photosphere (Fig. 3b);
- the angle γ between the LOS and $\boldsymbol{B}$ and the azimuthal angle χ are taken into account exactly, they depend on the height and distance from the axis (Fig. 3c).

We note the importance of the exact treatment of the angles for the realistic modeling. The geometrical path of the ray through the MFT can be divided into two parts: from the entrance into the MFT to the center and from the center to the exit (Fig. 3b). The contribution to the Stokes V signal is different for both parts. The second part is geometrically longer than the first and with the inclination γ smaller than the heliocentric angle θ resulting in a stronger contribution to Stokes V. Yet, the first part of the path is short but can have a "neutral line" (no contribution to V) and even can have a negative contribution to the emergent V signal ($\gamma > 90°$) (Fig. 3c). Moreover, numerical tests have shown that for strongly inclined magnetic fields (MFTs at the limb) due to the magneto-optical effects the Stokes V signal also depends strongly on the azimuthal angle χ.

To provide a satisfactory precision of the integration an irregular adaptive grid along each ray was used and the optical step size $\Delta\log(\tau) = 0.1$ was not exceeded. To account for the contribution of optically thin MFTs to the integration, flux tubes contain at least five grid points (Figs. 3c-d). The physical conditions inside a MFT differ strongly from that in the ambient plasma. This leads in the numerical model to an abrupt jump of the integrand on the boundary of MFTs. For a sufficiently accurate treatment of the jump two additional grid points were introduced at the boundary, separated by a very small distance, which gives negligible contribution to the integration (Fig. 3d).

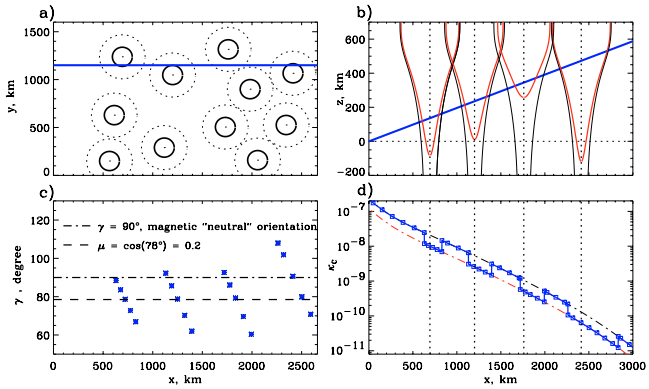

Fig. 3. Geometry of a ray crossing several flux tubes at $\mu = 0.2$ in the X-Y plane **a)** and the X-Z plane **b)**. Panel **c)**: angle between $\boldsymbol{B}$ and LOS as a function of spatial position; dashed: for purely vertical magnetic fields; dashed-dotted: magnetic field oriented perpendicular to the LOS; asterisks: inclination angles at grid points inside the MFTs. Panel **d)**: continuum opacity $\kappa_{\rm C}$ (in cm^{-1}) along the integration path (solid line) consisting of $\kappa_{\rm C}^{\rm int}$ (dotted dashed line) on the path through the MFTs and of $\kappa_{\rm C}^{\rm ext}$ (dashed line) elsewhere; vertical dotted lines show the locations of the flux tube centers **b)**.

The spacing between the rays is 25 km (~0.″035) in both X and Y directions. Such a high resolution of the model was provided at the expense of high computational demands.

For the adopted size of the simulation box of $3'' \times 2''$ such a resolution requires approximately 6000 individual rays at $\mu = \cos\theta = 1.0$ and even more at larger heliocentric angles θ. The rays which are strongly inclined to the vertical direction require a larger horizontal extent of the simulation box to account for the increased geometrical path of the rays along the LOS.

2.4. Atmospheric parameters and radiative transfer in a magnetized atmosphere

The atmosphere of each of the two components of the model (internal end external) is described by gas pressure and temperature stratifications ($P_{\rm g}, T$) as functions of geometrical scale z. However, to solve the radiative transfer equation, we need to know for each component several physical quantities such as continuum opacity, which requires the knowledge of the electron pressure, the partial hydrogen pressure, and the line opacity, i.e. the number density of the absorbers. All model calculations were made under the assumption of *local thermodynamical equilibrium* LTE, following the recipes of Aller (1963), Landi Degl'Innocenti (1976, 1992) and Rees et al. (1989).

For the numerical integration of the radiative transfer equation (RTE) we used the **DELO** (**D**iagolal **E**lement **L**ambda **O**perator) method by Rees et al. (1989) with a linear interpolation between grid points. This numerical scheme provides a fast and accurate solution of the RTE. The **DELO** method was programmed and its accuracy was tested by computing the

intensities for cases in which an analytical solution of the transfer equation is known.

The spectral lines under study (Fe I 6301.5 Å, 6302.5 Å and Fe II 6149.3 Å) were synthesized by solving the RTE along rays through the inhomogeneous model atmospheres at different wavelength positions. Oscillator strengths given by Thévevin (1990) were used. The additional broadening of the Stokes profiles caused by the macroturbulence was performed in the usual way by the convolution of synthetic line profiles with a Gaussian function of a width given by the macroturbulence velocity $v_{\rm mac}$. We used the constant value of $v_{\rm mac} = 1.25\ {\rm km\,s^{-1}}$ throughout, in both the MFT and the ambient atmosphere.

In order to calibrate our numerical model and to test the accuracy of the RT code and spectral line synthesis, we calculated Stokes I profiles from the average photospheric model VALC (Vernazza et al. 1981) and compared them to the averaged observed profiles from the Fourier Transform Spectrometer (FTS) Atlas by Brault & Neckel (cited by Neckel 1999). A satisfactory fit was achieved. Similar to Pérez Rodríguez & Kneer (2002) we found that in order to fit the wings of the synthetic spectral lines to the reference ones some enhancement factor to the damping constant C_6 (Unsöld 1955) in the range of 2–5 is required.

We note that the adopted LTE assumption is best fulfilled in the lower levels of the photosphere where the density is relatively high and the collisions control the energy distribution. The spectral lines used in this work originate from the heights where the LTE assumption is valid, except for the region of the line core formation of the strong Fe I 6301.5 line. The latter is formed in the upper layers of the solar photosphere (up to $z \sim 500$ km) where NLTE effects become significant (Shchukina & Trujillo Bueno 2001). However, in the modeling performed for this study all NLTE effects were neglected.

In order to simulate the limited spatial resolution of the observation caused by the diffraction limit of the telescopes and *seeing* conditions the synthetic 2D maps for each wavelength position were convolved with Gaussian functions to produce spatial resolution of 0.25″, 0.5″ and 1.0″, which approximately correspond to the spatial resolutions of our data observed in the broadband channel of the FPI in the VTT (speckle reconstructed), in narrowband of the FPI (deconvolved with the instantaneous OTF) and to the moderate resolution of the 1D spectrograms observed with GCT, respectively (Paper I).

For comparison with the FPI observations the calculated intensity profiles were additionally convolved in wavelength with the Airy function of the spectrometer.

2.5. Internal thermal model

Temperature is a determining factor in the process of spectral line formation, which affects many observed properties of intensity profiles such as Doppler width, continuum and line core contrasts, line depression, and amplitudes of polarimetric signal. Therefore, an adequate choice of the temperature stratification inside flux tubes is an important aspect of the numerical modeling and radiative transfer calculations.

A realistic temperature model can be found either from a solution of a system of MHD equations (e.g., Keller et al. 2004, and references therein), or by means of inversion of high resolution spectroscopic data observed in facular structures, or from the analysis of the CLV of the intensity contrast. In the forward modeling which is performed in this work the temperature stratification cannot be obtained consistently from some equations. It is a free parameter of the model, which should be prescribed independently of other model parameters. Therefore, we need to define a reasonable temperature as a function of height $T(z)$ inside a single magnetic flux tube.

From the analysis of the observations (Paper I) it was found that the iron lines observed in PFe possess several peculiar features that strongly distinguish facular atmospheres from the surrounding quiet photosphere, and which are very likely due to the thermal structure of the faculae:

- strong contrast both in the continuum and line core for all three lines;
- in the Fe II 6149.3 line the Stokes I profiles from PFe ($I_{\rm PF}$) are substantially stronger and broader than the averaged intensity profile from the surrounding quiet Sun photosphere $I_{\rm QS}$;
- in the Fe I 6301.5 line $I_{\rm PF}$ show almost the same line depression as $I_{\rm QS}$ but appear to be slightly broader than $I_{\rm QS}$;
- in the Fe I 6302.5 line $I_{\rm PF}$ are weaker and broader than $I_{\rm QS}$.

These properties were found from the observations without any exceptions and so such behavior seems to be inherent to the facular atmospheres. Therefore, they were used as a criterion to choose the most plausible thermal model of the flux tube atmosphere for further model calculations.

It is generally accepted that strong magnetic fields inhibit convective energy transport, resulting in a reduced temperature inside a MFT at any geometrical height. Such a model is called a *hot wall* model and was first proposed by Spruit (1977) and later developed by Deinzer et al. (1984). The *hot wall* concept is often used to explain the observed CLV of the continuum brightness of plage faculae.

An alternative mechanism (*hot cloud* model) of the increased facular contrast at large heliocentric angles was suggested by Knölker et al. (1988). In the *hot cloud* model, flux tubes are characterized by some temperature excess in the upper layers of the photosphere. This is due to the lateral influx of heat by horizontal radiative transfer in the medium with strong horizontal pressure gradients. It was shown by Fabiani Bendicho et al. (1992), who have performed 2D numerical radiative transfer calculations, that for thin flux tubes, radiation channeling leads to an enhancement of the temperature of the upper layers. Later, Bellot Rubio et al. (2000) found from the inversion of spectra from plage faculae that flux tube atmospheres are cooler than the ambient gas at heights below $z = 0$ km and hotter at $z > 0$. Eker (2002) presented a comprehensive study of various cloud models of solar faculae as plane parallel structures above the photosphere and their influence on the center-to-limb variations of the intensity contrast.

Both temperature models, *hot wall* (HW) and *hot cloud* (HC), were adopted in our modeling as reference thermal stratifications. To construct a HW model with a flux tube

cooler at all geometrical heights we have shifted $T(z)$, given by the VALC model, downward by a Wilson depression of $\Delta z = 100$ km. The choice of the HC stratification is arbitrary with cooler T at $z < 0$ km and hotter T at $z > 0$ km.

Some comments about the HW model are appropriate. Hot walls, exposed to an optically thinner medium, become cooler through the channeling effect (Cannon 1970). A model for the convective and radiative energy transport near the wall is needed to get the wall contributions to the emergent intensity correct. A two-dimensional parameter study of the radiative energy flux through embedded magnetic flux features was performed by Fabiani Bendicho et al. (1992, see also references to earlier work therein). Two-dimensional MHD modeling of flux sheets by, e.g., Steiner (2005 and references therein) demonstrate that the cooling of the walls causes a down flow in the medium surrounding the magnetic feature and, important in this context, a depression of the continuum intensity centrewards of the flux sheet. Fully three-dimensional MHD simulations by Keller et al. (2004) show the same decrease of intensity as narrow dark lanes in front of the bright faculae, as observed, while the hot wall effect remains.

Taking the hot wall from the unperturbed subphotospheric medium overemphasizes its contribution to the facular intensity. Steiner (2005) and Carlsson et al. (2004) discuss facular intensities on the basis of two- and three-dimensional MHD simulations, respectively. On the one hand, the hot walls cool down through radiative energy transport into the MFTs. On the other hand, the heat is efficiently replenished by convection and the energy flow into the flux tubes heats their deep atmospheres, which partially counteracts the lowering of the wall intensity by cooling. The contribution of the MFTs to the facular intensity is important especially when many MFTs are crossed by the light rays as in our modeling of PFe. We defer the inclusion of a medium cooler than the hot, normal (sub-)photosphere to a further study.

For each of the above temperature models a corresponding flux tube atmosphere was generated taking into account a partial evacuation of the tube in accordance with the pressure balance (Sect. 2.2). For the thus created flux tube atmospheres and for the quiet Sun (VALC) synthetic Stokes I and V profiles were calculated. In order to find out how the partial evacuation of the MFT and different temperature stratifications change the heights of the spectral line origin the corresponding contribution functions (CF) to the line depression were calculated.

Calculated Stokes profiles together with corresponding CF were analyzed for each model (Okunev 2004). We found that it was difficult to reproduce all observed properties of Stokes I profiles for the three spectral lines under consideration using either one of the above temperature models, HW or HC. Depression and contrasts of the ionized iron line are explained better by the HW model, while for the spectral lines of neutral iron the adopted HC model is more preferable.

The sought temperature stratification was deduced in few iterations by manual adjustment of the initial temperature curves and by comparison of the properties of the synthetic line profiles with the observed ones. The thermal model obtained in this way, with $T_{\rm int}(z < 120) < T_{\rm VALC}$ and $T_{\rm int}(z > 120) > T_{\rm VALC}$, is presented in Fig. 4 (thin solid line). We compare it with the internal temperature obtained by Bellot Rubio et al. (2000) by means of inversion of Stokes profiles emerging from plage regions (Fig. 4 dashed line). They agree well in the range of heights from −100 km to 300 km.

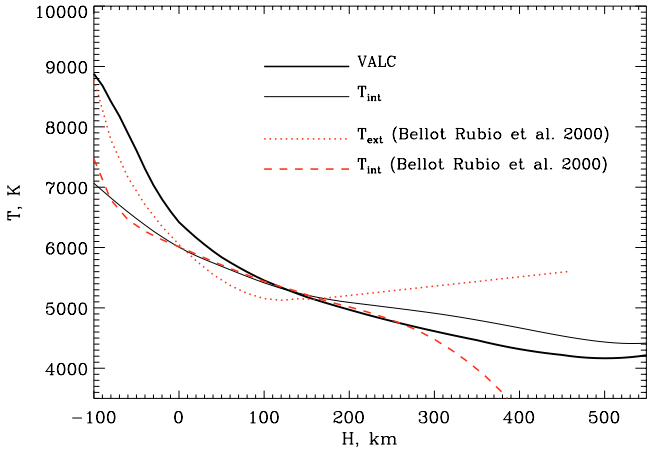

Fig. 4. Used internal temperature model (thin solid line) and the VALC temperature (thick solid line) compared with internal (dashed line) and external (dotted line) temperature obtained from inversion of Stokes profiles by Bellot Rubio et al. (2000).

The deduced model successfully reproduces depressions, continuum and line core contrast in spectral lines of both neutral and ionized iron and therefore it is an appropriate choice of a temperature stratification inside MFTs to be used for the radiative transfer calculations.

3. Results of numerical modeling and comparison with observations

3.1. Effect of many MFTs along the ray

Magnetic flux tubes are tiny structures in the solar atmosphere. At the photospheric level of $z = 0$ km they have a diameter $d \sim 200$ km or even smaller. Although they expand upwards, reaching $d = 1'' \sim 700$ km in higher layers of the photosphere, they still remain optically thin structures with a small contribution to the emergent intensities.

However, it was found from the observations that intensity profiles from PFe differ strongly in many characteristics from the averaged profiles from the surrounding quiet atmosphere. To produce such effects the MFTs, which constitute PFe, should have a large contribution along the integration path, which in turn can be ensured only by a sufficiently large number of small-scale MFTs traversed by the rays in the resolution element.

In order to study the effect of the number of MFTs along the integration path on the photometric and spectropolarimetric properties of the radiation from magnetic elements we have fixed all the free parameters of the model (line λ6302.5, $\mu = 0.2$, $B_0 = 1400$ G, $R_0 = 100$ km), and have varied only the number of flux tubes in the simulation box. For the three earlier adopted random distributions of the MFTs on the surface (N1, N2, N3, see Table 1) numerical modeling and radiative transfer calculations were performed. The synthetic intensity

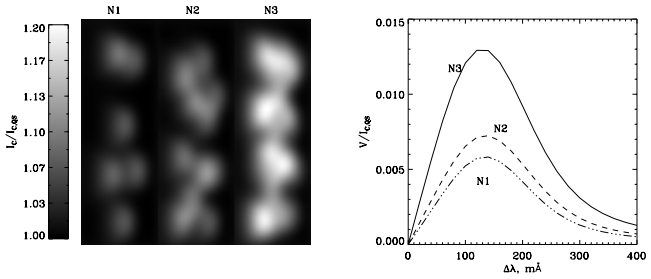

Fig. 5. *Left panel*: continuum intensity maps calculated at $\mu = 0.2$ from the three realizations of the MFTs on the surface. The image sizes are $0.7'' \times 2''$. *Right panel*: red lobes of the corresponding Stokes V signals of the λ6302.5 line.

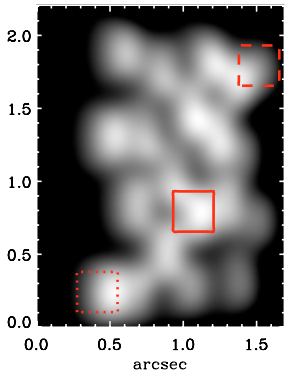

Fig. 6. Synthetic continuum intensity map at $\mu = 0.4$. Solid, dashed and dotted squares show the regions over which the intensity profiles of Fig. 7 were averaged. Limb side is left.

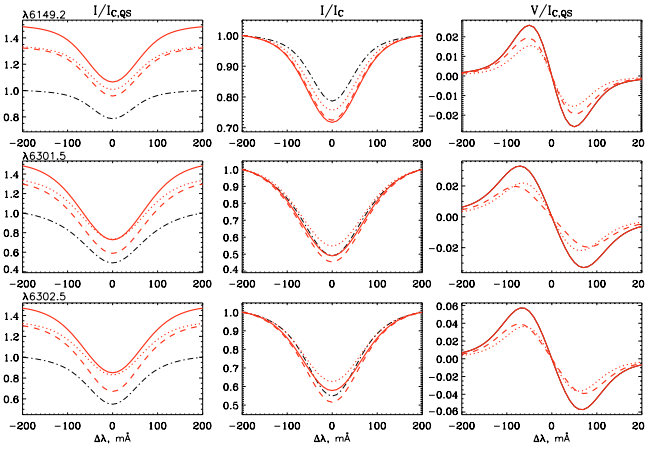

Fig. 7. Spectropolarimetric profiles from synthetic facula at $\mu = 0.4$. Solid, dashed and dotted profiles emerge from the regions (1), (2) and (3) presented in Fig. 6 as squares with corresponding line types. Dashed-dotted lines correspond to profiles from the ambient quiet Sun.

maps were convolved with a smearing function simulating limited spatial resolution (seeing ~0.3″).

It can easily be seen (Fig. 5) that the distributions N1 and N2 produce very low contrasts and weak V amplitudes, and therefore are not appropriate for the modeling of PFe. The most populated distribution N3 ($N_{\rm MFT} = 21$, $f_{\rm mod} = 0.2$, Sect. 2.3) produces more reasonable characteristics of the intensity profiles, although the amplitudes and contrasts are still slightly weaker than the strongest observed in PFe. To achieve a better correspondence of the synthetic faculae with the typically observed ones, another free parameter of the model R_0 can be used to tune the model and to control the contribution of the MFTs to the emergent intensity. After several numerical experiments it was found that by adopting the flux tube radius R_0 in the range from 100 km to 150 km a good agreement with the observations can be achieved.

3.2. Spectropolarimetric profiles from synthetic faculae

In this section we compare observed and calculated spectropolarimetric profiles from faculae close to the limb.

The synthetic Stokes I and V profiles were obtained with the following model parameters: $\mu = 0.4$, $B_0 = 1400$ G, $R_0 = 150$ km and distribution N3. The spatial resolution of 0.5″ and spectral resolution of ~40 mÅ were simulated in accordance with the parameters of observations in the narrow band of the Fabry Perot spectrometer in the VTT.

The spatial size of the synthetic data cubes $I(x', y', \lambda)$ and $V(x', y', \lambda)$ is $2.2'' \times 1.7''$. Obviously, the properties of I and V profiles depend on the spatial position $\{x', y'\}$ in the simulated intensity pattern, because each individual ray has different contributions to the emergent intensity from the MFTs along the integration path. For demonstration purposes three regions in the intensity map were selected (Fig. 6), over which the Stokes I and V profiles were averaged:

1) the region containing the brightest point in the middle of the cluster with a large contribution of MFTs along the LOS, both line core and continuum intensities are formed within flux tubes (solid square in Fig. 6);
2) the region at the center side of the cluster, the line core is formed in the non-magnetic plasma, the continuum in a magnetically intermittent atmosphere (dashed square);
3) the region at the limb side of the cluster, the line core is formed in an intermittent photosphere, the continuum in the non-magnetic plasma (dotted square).

The Stokes I and V profiles synthesized in three spectral lines were averaged in each of the selected regions. Their properties (continuum and line core contrasts, depressions of I and amplitudes of V) were compared with each other and with profiles from the surrounding quiet Sun as shown in Fig. 7.

Middle of facula. Region 1. The intensity profiles (solid lines in Fig. 7) have the highest contrasts in continuum and in line core, and also possess relatively strong V amplitudes. The depressions of the I profiles from the brightest point in the synthetic facula are close to those calculated under the assumption of a plane-parallel atmosphere with a ray staying always in a flux tube atmosphere. All these effects are due to the large contribution of MFTs along the integration path to the intensities emerging from the middle of the apparent intensity pattern.

Profiles from the center side and the limb side are formed in the magnetically intermittent atmospheres, and therefore they exhibit a different behavior.

Center side. Region 2. The profiles (dashed lines) possess smaller contrasts at line cores compared to the region 1, because the core intensities at the limb side are formed under conditions close to the external VALC photosphere. In the case

of λ6149.3 the line core contrast is still strong due to the low levels of formation which are more effected by the flux tube component than the upper layers where the cores of neutral iron lines are formed. The continuum contrast is weaker than from region 1, due to the decreased contribution from MFTs along the rays in the resolution element compared to region 1. The Stokes V profiles are weaker than from region 1 for the same reason. The depressions of the neutral iron lines are larger. This is due to the increased difference of heights (accordingly higher temperature difference) between the regions of continuum and line core formation.

Limb side. Region 3. The line core contrasts from the limb side (dotted lines) are similar to those from region 1. In both cases the line core radiation originates from approximately the same heights in the flux tube interior, while the continuum intensities are formed under different conditions. The continuum contrasts and V amplitudes are weaker due to the small contribution of MFTs along the LOS. The line depressions are weaker, because line core and continuum are formed in a narrower range of heights with smaller temperature difference.

In this way it was found that spectral properties of the radiation from facular structures observed close to the limb are very much influenced by the magnetic intermittency of the atmosphere along the LOS. For the adopted model at $\mu = 0.4$ with $R_0 = 150$ km and rich populated with MFTs (distribution N3) the contribution from individual flux tubes is dominant in the middle of the simulated intensity pattern, however at the limb and central sides the inhomogeneity of the atmosphere results in a strong variation of the properties of the I and V profiles.

The simulated profiles agree well with the observations (Paper I). Contrasts, depressions, intensity profile variations are well reproduced.

3.3. Spatial distribution and fine structure

In this section we test the ability of the numerical model to simulate some of the apparent properties of PFe, such as fine structure, sizes and spatial distribution of the brightness and polarimetric signal.

For the comparison with the observations we have chosen a model with the following parameters: $B_0 = 1400$ G, $R_0 = 100$ km, MFT distribution N3, $\mu = (0.4, 0.2, 0.1)$. A spatial resolution of $0.3''$ was simulated. The emergent Stokes profiles were convolved with the Airy function of the FPI spectrometer in order to simulate the limited spectral resolution of the observations. The apparent spatial distribution of the apparent LOS magnetic field was obtained by estimating the amplitudes of the Stokes V profiles in the λ6302.5 line. The intensity maps calculated in the continuum close to the spectral lines (Fig. 8) are very similar to the ones observed with high spatial resolution (Paper I).

It was generally found that several apparent properties of the simulated structures are in a good agreement with the observations:

- high intensity contrasts, decreasing towards the extreme limb;

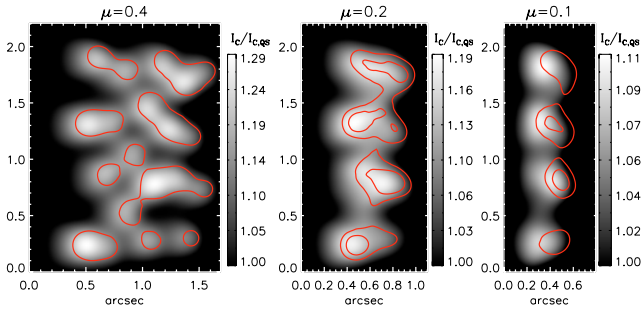

Fig. 8. Synthetic continuum intensity maps normalized to the intensity of the surrounding quiet Sun and overplotted with the contours of the LOS magnetograms. Left side of the maps corresponds to the direction to the limb.

- at $\mu = 0.4$ the synthetic polar faculae appear as a cluster with a complex fine structure (subarcsec sizes) both in brightness and magnetic field strengths;
- at $\mu = 0.2$–0.1 they consist of small bright structures organized in chains stretched parallel to the limb, the distance between the pearls in the chain is about $0.5''$;
- the distribution of the polarimetric signal is shifted towards disk center with respect to the continuum brightness.

The similarities with the observed PFe and their fine structure and sizes are based on the adopted concept of small-scale MFTs. But the ability of the model to reproduce the observed spatial shifts of polarimetric signal with respect to continuum intesity (Paper I) is remarkable. It demonstrates the reliability of the constructed model. We note that such shifts are also visible in Steiner's (2005) numerical simulations, but with a very small amount, presumably due to the limitations in the presentation (his Fig. 5) to $\mu = 0.5$. The interpretation of the observed shifts without numerical simulation would not be straightforward because, as it was shown in the previous section, the amplitudes of the V signal depend not only on field strengths and inclinations but also on the temperature along the LOS in a non-trivial way. Temperature affects opacities (height of formation), line strength and Doppler width of the lines, which in turn affect the Stokes V signal. The enhancement of the brightness can be due to the reduced opacity along the LOS, which allows to see deeper and hotter layers of the photosphere. The numerical model considers all the effects in a consistent way and successfully simulates the observed properties of PFe.

3.4. Center-to-limb variation of brightness contrast and of Stokes V amplitudes

We now test ability of the models to reproduce the CLV of the brightness contrast defined as $(I_{\max}(\mu)/I_{\mathrm{VALC}}(\mu) - 1) \times 100$ and of the Stokes V amplitudes. In the observations, no maximum of the apparent contrast in the observed range of heliocentric angles ($\mu = 0.4$–0.1) was measured. A similar behavior was found in the CLV of the Stokes V amplitudes.

The radiative transfer calculations for each simulation box were performed for several inclinations of the LOS to the vertical axis of the model. Calculations were performed for R_0 equal to 100 km and 150 km, and for MFTs distributions N2 and N3

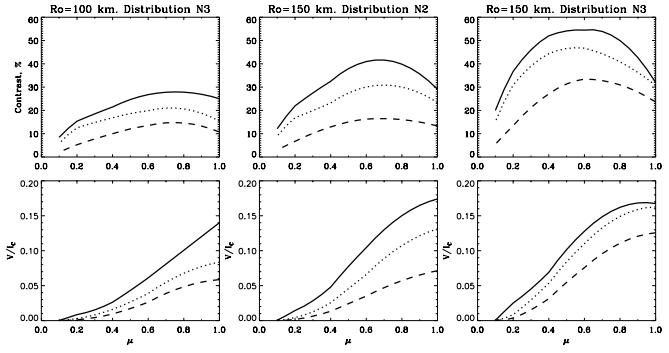

Fig. 9. CLV of the continuum intensity contrast and the Stokes V amplitude in the λ6302.5 line for three different models. Solid, dotted and dashed lines denote the spatial resolution of 0.″25, 0.″5 and 1″, respectively.

(Sect. 2.3). The Stokes V amplitudes were derived from the polarimetric signal in the λ6302.5 line.

The resulting center-to-limb variations are presented in Fig. 9. It was found that the shape of the CLV curve is very sensitive to the parameters of the model and above all to the resolution of the observations. Convolution with a smearing function not only systematically reduces the contrast but also changes the shape of the CLV, and particularly can change the position of the maximum of the intensity contrast. We found that the position of the maximum of the continuum intensity contrast for the adopted model is in the range of $\mu = 0.4{-}0.7$ depending on the free parameters and the spatial resolution.

The model with $R_0 = 100$ km (Fig. 9, left panels) results in intensity contrasts of 20−30% near the limb which are approximately two times weaker than the observed values. The model with $R_0 = 150$ km produces contrasts closer to the observed. The increase of the number of MFTs (from N2 to N3) along the rays in the resolution element moves the position of the maximum towards the limb and leads to a substantial enhancement of the apparent brightness near the limb, though the contrast at disk center ($\mu = 1.0$) is less sensitive to this parameter of the model (Fig. 9, right panel).

Comparing the simulated CLV with the observed ones we can conclude that the model with ($T_{\rm int}$, $R_0 = 150$ km, N3) results in properties that are closest to the observed. However, although the CLV of the synthetic PF intensities demonstrates trends similar to the observed, no perfect correspondence to the observations was achieved. This can be due to the fact that our model is limited to two components, internal and external, with the external atmosphere prescribed by the VALC model. More realistic calculations of the CLV of the contrast should take into account more components of the photosphere (granule, intergranule, facula interior and exterior atmospheres). In addition, variable sizes of MFTs within one facula, i.e. size distributions, need also to be considered in further simulations. An ensemble of structures of different sizes will exhibit a different CLV than a single-sized ensemble (cf. Spruit 1976). The potential value of such calculations lies in the determination of the *size distribution*. Using distributions will result CLVs much sharper peaked near the limb, which however has not been observed for PFe (cf. Paper I) nor been found in Steiner's (2005) two-dimensional MHD simulations of magnetic flux sheets.

3.5. Apparent magnetic field strength

Several calibration techniques can be used for an estimation of the apparent magnetic field strengths in solar faculae. These approaches are based on several assumptions which simplify the interpretation of the observations and allow to estimate physical quantities without involving complicated radiative transfer calculations. Yet, the question whether the adopted assumptions are valid for the observations near the limb, where the magnetic field is very intermittent along the LOS, still remains open.

The performed modeling makes it possible to verify the reliability of the used calibrations and to test the validity of the underlying assumptions. The parameters of the used model are: $T_{\rm int}$, $R_0 = 150$ km, $B_0 = 1400$ G at $z = 0$ km, distribution N3, $\mu = \cos\theta = 0.4$, spatial and spectral resolution of the Fabry-Perot spectrometer in the VTT (narrowband). The output from the model calculations are the synthetic data cubes $I(x', y', \lambda)$ and $V(x', y', \lambda)$, where x' and y' are coordinates in the plane perpendicular to the LOS. In this section we apply exactly the same methods to the synthetic data cubes as were applied to the observed data sets (Paper I).

First, we compare the relation between separations and amplitudes of synthetic Stokes V lobes with the observed relation. The simulated diagram of $\Delta\lambda_V$ vs. $V_{\rm amp}$ (right panel of Fig. 10) is in very good agreement with the observations from PFe. The ranges of the calculated and measured values and the triangular shape of the relation between the separations and amplitudes are very similar.

In order to estimate the apparent magnetic field strengths from the synthetic profiles we have used two approaches:

- from the amplitudes of Stokes V in the weak field approximation (WFA);
- from the separations of the Stokes V extrema, i.e. assuming the strong field regime.

In the weak field approximation the magnetic field was estimated from the synthetic polarimetric signal in all three spectral lines used for the observations (Fig. 10 left panel). The obtained values are much smaller than the intrinsic kilo-Gauss fields of the model, because the method gives only the LOS component of the average magnetic flux density $B_{\rm WFA} = fB\cos\gamma$. The values obtained from the synthetic λ6149.3 and λ6301.5 lines are close to each other and to the values obtained from the observation with the Fabry-Perot spectrometer in the VTT. As expected, for the λ6302.5 line the WFA approximation is not at all valid for PFe, this line is very sensitive to the magnetic field, it enters the strong field regime already for 1 kilo-Gauss fields, and Stokes I exhibits non-negligible Zeeman broadening.

The histogram of the magnetic field strength derived from separations of the synthetic Stokes V lobes in the Fe I 6302.5 line assuming the strong field regime (Fig. 10 middle panel) is in good agreement with the real field strengths adopted in the numerical model ($B_0 = 1400$ G). Also the

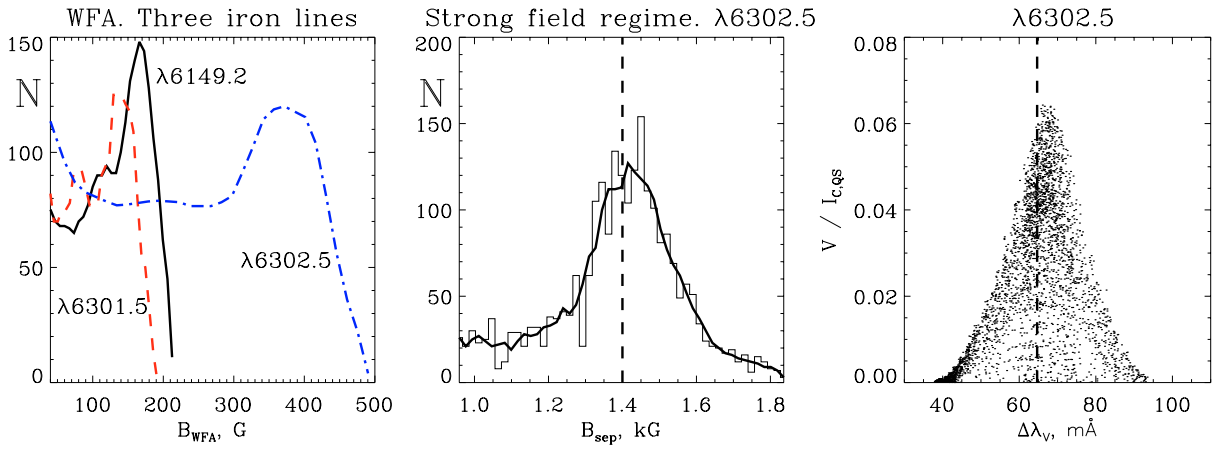

Fig. 10. Estimation of the apparent magnetic field from the synthetic data cubes $I(x', y', \lambda)$ and $V(x', y', \lambda)$. *From left to the right*: histogram of the average flux density calculated from the WFA; histogram of magnetic field strength calculated from the separations of the V extrema; diagnostic diagram: amplitudes vs. separations. The value of the true intrinsic magnetic field (parameter of the model B_0 = 1400 kilo-Gauss) is shown by the vertical dashed line.

shape of the curve and the range of field strengths are similar to the distribution of the magnetic field strengths measured in PFe on the Sun. We conclude that this method is less sensitive to the area filling factor and inclination of the magnetic field. However, this technique tends to overestimate the field strength. Some V profiles have very large separations, resulting in a long tail of the distribution in the middle panel of Fig. 10 which reaches apparent fields of 2 kilo-Gauss, strengths which are not present in the adopted model at the heights of formation of this spectral line. This peculiarity was noted also in the observational data (Paper I).

A close inspection of the model allows us to explain this effect. Magnetograms calculated from the amplitudes and the separations have very different spatial distributions as shown in Fig. 11. Note that in this figure the primary information, the magnetic field signals, are given in grey scale, while the intensity pattern showing the location of the facula is overlaid by the contours. The Stokes V amplitudes, apart of the above mentioned small shift towards the center, coincide in general with the intensity pattern, but the separations do not. The most strongly separated V profiles originate from the extreme center side of the simulated pattern. They correspond to the special case when the core of a spectral line is formed in a non-magnetic atmosphere, while the intensities at spectral position close to the continuum emerge from the magnetic plasma. The corresponding Stokes V profiles will have no signal at wavelengths close to the line center, and will have weak lobes near the continuum of the spectral line. In such a way, the wide separation of the V lobes does not reflect a strong magnetic field at the heights of formation, but is simply a consequence of the intermittent magnetic field along the LOS.

The most separated V profiles are characterized by very weak V signal, which is below the noise level and therefore they are not detected. However, slightly less separated profiles have accordingly stronger V amplitudes which can be detected. Such profiles result in long tails of the observed distributions.

In this way from the comparison of the properties of the observed and calculated polarimetric signals and of apparent

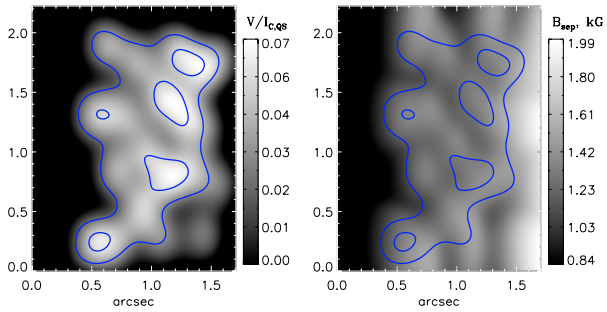

Fig. 11. *Left panel*: amplitudes of the synthetic Stokes V signal. *Right panel*: apparent magnetic field measured from the separation of the V lobes. Both maps are over-plotted with the contours of the continuum brightness.

magnetic field found in synthetic and observed faculae we conclude that:

1. the created numerical model with the adopted set of free parameters adequately simulates the properties of the Stokes V signal, apparent magnetic field strengths and average flux density of polar faculae on the Sun, which confirm the reliability of the model;
2. magnetic field determination close to the limb in WFA is valid when applied to proper spectral lines with $\Delta\lambda_D \gg \Delta\lambda_V$, yet this method estimates only the average magnetic flux density in the LOS direction, which strongly depends on the spatial resolution of the observations and on the inclination of magnetic field;
3. magnetic field determination assuming the strong field regime gives reasonable values of magnetic field strength, it is less sensitive to inclinations and area filling factor, however it should be applied with some care to data obtained near the solar limb. This method can overestimate the real field strength when radiation emerges from atmospheres which are magnetically inhomogeneous along the LOS.

4. Conclusions

In this section we briefly summarize the main results from the numerical simulations. A realistic numerical model of facula structures observed at large heliocentric angles was created. The model has two components: small-scale magnetic flux tubes embedded in a field-free plasma, and is controlled by several free parameters. The magnetic intermittency of the facula atmosphere along the LOS was taken into account consistently.

By varying the free parameters of the model a good agreement of the characteristics of synthetic faculae to the characteristics of the observed polar faculae was achieved.

The created numerical model successfully reproduces the following quantitative and qualitative properties of radiation from PFe:

- ⋆ enhanced intensity contrasts of facular structures at the limb;
- ⋆ fine structure in brightness and magnetic fields;
- ⋆ sizes and shapes of PFe;
- ⋆ spatial distribution of apparent magnetic field in PF: the maximum of the polarimetric signal is shifted towards the disk center with respect to facular brightenings in continuum;
- ⋆ trends and general properties of the center-to-limb variation of continuum intensity contrast and Stokes V amplitude;
- ⋆ peculiar spectropolarimetric behavior in all spectral lines under study: depressions and line core contrast in Stokes I profiles and amplitudes and separations of V;
- ⋆ apparent kilo-Gauss magnetic field strength and average flux density estimated in weak field approximation;
- ⋆ model reproduces and allows us to explain the observed widely separated Stokes V lobes with $\Delta\lambda_V > 90$ mÅ.

We summarize the obtained parameters of the numerical model, which produce the similarities listed above with observations:

- A large number of magnetic flux tubes along the LOS is required to reproduce the observed intensity contrasts and amplitudes of the polarimetric signal. The distribution N3 ($N_{\rm MFT} = 21$ in the simulation box, $f_{\rm mod} = 0.2$, Sect. 2.3) was adopted.
- A magnetic field strength $B_0 = 1400$ G at $z = 0$ km was found to be an adequate choice of this free parameter of the model and it was used throughout the study. This value is in good agreement with the result of the inversion of Stokes profiles from plage regions performed by Bellot Rubio et al. (2000).
- The radius of a MFT at the surface R_0 was chosen to be in the range 100−150 km. Such values are a compromise between the required large enough contribution from optically thin MFT to the emergent intensities and the fine structure of facula elements.
- Spectral and photometric properties of radiation are very sensitive to the adopted thermal model of the flux tube interior. Starting with the initial temperature stratifications (*hot wall* and *hot cloud*) and comparing the synthetic intensity profiles with the observed ones in three iron lines, we have deduced a temperature model with $T_{\rm int}(z < 120) < T_{\rm VALC}$ and $T_{\rm int}(z > 120) > T_{\rm VALC}$, which results in a good agreement of synthetic profiles with observations in all three lines simultaneously. This temperature stratification of the flux tube interior agrees well with results of inversion of Stokes profiles (Bellot Rubio et al. 2000). Thus, the deduced model is an appropriate choice of temperature stratification inside MFTs for the performed simulations with the adopted model assumptions, i.e. two components and fixed parameters of the external atmosphere.
- Apparently, this temperature structure is a combination of the *hot wall* model and the *hot cloud* model. The former is appropriate in explaining the continuum intensities (e.g., Keller et al. 2004) and low forming spectral features, while the latter, with its low temperature gradient, is needed to reproduce the spectral features formed at higher layers.

The ability of the adopted numerical model with a reasonable choice of parameters to reproduce and explain the observed properties of polar faculae proves the reliability of the hypothesis that PFe consist of concentrations of small-scale kilo-Gauss magnetic flux tubes.

The constructed model is controlled by several free parameters and therefore can be used for the interpretation of the polarimetric observations at large heliocentric angles and for verification of different calibration techniques used for data analyses.

For simplicity the model was limited to the two-component (internal and external) case with static magnetic flux tubes and zero macroscopic velocities. Therefore, an obvious improvement to the model would be to abandon the above simplifications:

- radiative transfer calculation in the simulation box with a predefined 3D velocity field will allow us to simulate in a realistic way the asymmetries of Stokes I and V profiles and upflows found in PFe;
- a model with more components (granule, intergranule, faculae interior and exterior atmospheres) and with variable sizes of magnetic flux tubes within one facula should provide a better correspondence of individual synthetic intensity profiles to the observed ones and also improve the synthetic center-to-limb variation of the continuum intensity contrast;
- selfconsistent dynamical modeling is needed to simulate the time evolution of PFe.

The latter two improvements can be achieved only by combination of realistic magneto-hydrodynamic simulations, as carried out, e.g., by the Lindau-Chicago group (Vögler et al. 2005), with radiative transfer calculations at large heliocentric angles.

Acknowledgements. Most of this work was accomplished while OO was visiting the Universitäts-Sternwarte Göttingen, supported by the *German Academic Exchange Service – DAAD* through grant A/00/01395. He thanks the Universitäts-Sternwarte Göttingen for the hospitality.

References

Aller, L. H. 1963, Astrophysics. The Atmospheres of the Sun and Stars, 2nd ed. (New-York: Ronald Press)

Audic, S. 1991, Sol. Phys., 135, 275

Bellot Rubio, L. R., Ruiz Cobo, B., & Collados, M. 2000, ApJ, 535, 489

Borrero, J. M., & Bellot Rubio, L. R. 2002, A&A, 385, 1056

Bünte, M., Solanki, S. K., & Steiner, O. 1993, A&A, 268, 736

Cannon, C. J. 1970, ApJ, 161, 255

Carlsson, M., Stein, R. F., Nordlund, Å., & Scharmer, G. B. 2004, ApJ, 610, L137

Deinzer, W., Hensler, G., Schüssler, M., & Weisshaar, E. 1984, A&A, 139, 435

Eker, Z. 2003, Sol. Phys., 212, 277

Fabiani Bendicho, P., Kneer, F., & Trujillo Bueno, J. 1992, A&A, 264, 229

Karpinsky, V., & Okunev, O. 1997, Sol. Phys., 173, 232

Karpinsky, V., & Okunev, O. 1998, Sol. Phys., 183, 277

Keller, C. U., Schüssler, M., Vögler, A., & Zakharov, V. 2004, ApJ, 607, L59

Knölker, M., Schüssler, M., & Weisshaar, E. 1988, A&A, 194, 257

Landi Degl'Innocenti, E. 1976, A&A, 25, 379

Landi Degl'Innocenti, E. 1992, in Solar Observations: Techniques and Interpretation, First Canary Islands Winter School, ed. F. Sánchez, M. Collados, & M. Vázquez (Cambridge UK: Cambridge Univ. Press), 77

Lites, B. W., Scharmer, G. B., Berger, T. E., & Title, A. M. 2004, Sol. Phys., 221, 65

Magain, P. 1986, A&A, 163, 135

Neckel, H. 1999, Sol. Phys., 184, 421

Okunev, O. V. 2004, Ph.D. Thesis, Göttingen University

Okunev, O. V., & Kneer, F. 2004, A&A, 425, 321 (Paper I)

Pérez Rodríguez, E., & Kneer, F. 2002, A&A, 395, 279

Pneuman, G. W., Solanki, S. K., & Stenflo, J. O. 1986, A&A, 154, 231

Puschmann, K., Ruiz Cobo, B., Bonet, J. A., Vázquez, M., & Hanslmeier, A. 2005, A&A, in press

Rees, D. R., Murphy, G. A., & Durrant, C. J. 1989, ApJ, 339, 1093

Ruiz Cobo, B., & del Toro Iniesta, J. C. 1992, ApJ, 398, 375

Shchukina, N., & Trujillo Bueno, J. 2001, ApJ, 550, 9706

Solanki, S. K. 1993, Space Sci. Rev., 63, 1

Solanki, S. K., Steiner, O., Bünte, M., Murphy, G., & Ploner, S. R. O. 1998, A&A, 333, 721

Spruit, H. C. 1976, Sol. Phys., 50, 269

Spruit, H. C. 1977, Ph.D. Thesis, Utrecht University

Steiner, O. 2005, A&A, 430, 691

Thévenin, F. 1990, A&AS, 82, 179

Unsöld, A. 1955, Physik der Sternatmosphären, 2nd ed. (Heidelberg: Springer), 333

Vernazza, J. E., Avrett, E. H., & Loeser, R. 1981, ApJS, 45, 635

Vögler, A., & Schüssler, M. 2003, Astron. Notes/AN, 324, 399

Vögler, A., Shelyag, S., Schüssler, M., et al. 2005, A&A, 429, 335